Supramolecular Recognition-Mediated Layer-by-Layer Self-Assembled Gold Nanoparticles for Customized Sensitivity in Paper-Based Strip Nanobiosensors

Xiaolin Huang, Yaofeng Zhou,* Lu Ding, Guocan Yu, Yuankui Leng, Weihua Lai, Yonghua Xiong,* and Xiaoyuan Chen*

Herein, a smart supramolecular self-assembly-mediated signal amplification strategy is developed on a paper-based nanobiosensor to achieve the sensitive and customized detection of biomarkers. The host–guest recognition between β-cyclodextrin-coated gold nanoparticles (AuNPs) and 1-adamantane acetic acid or tetrakis(4-carboxyphenyl)porphyrin is designed and applied to the layer-by-layer self-assembly of AuNPs at the test area of the strip. Thus, the amplified platform exhibits a high sensitivity with a detection limit at subattogram levels (approximately dozens of molecules per strip) and a wide dynamic range of concentration over seven orders of magnitude. The applicability and universality of this sensitive platform are demonstrated in clinically significant ranges to measure carcinoembryonic antigen and HIV-1 capsid p24 antigen in spiked serum and clinical samples. The customized biomarker detection ability for the on-demand needs of clinicians is further verified through cycle incubation-mediated controllable self-assembly. Collectively, the supramolecular self-assembly amplification method is suitable as a universal point-of-care diagnostic tool and can be readily adapted as a platform technology for the sensitive assay of many different target analytes.

1. Introduction

The presence of specific disease biomarkers in organs, tissues, bodily fluids, or cells is vital for disease diagnosis.[1] Early and timely detection of such biomarkers provides a promising and powerful method to improve disease diagnostics and to enable timely treatment.[2] Nevertheless, the concentrations of these available biomarkers, such as proteins, nucleic acids, lipids, metabolites, and cells, in diverse samples are found in a wide dynamic range, covering over six orders of magnitude from microgram per milliliter to picogram per milliliter or even lower.[3] Therefore, a sensitive biomarker detection technology that can cover a wide concentration range even at a trace level to allow the accurate and reliable determination of biomarkers will enable early diagnosis, dynamic monitoring, and prognosis evaluation.[3c,4] However, to our knowledge, no available universal diagnosis platform is suitable to overcome these challenges.

Paper-based strip nanobiosensors are one of the most prominent point-of-care diagnostic devices and have found use in a variety of applications in disease control, food safety, and environmental monitoring because of their simplicity, portability, rapidity, and low cost.[5] Traditionally, strip nanobiosensors generally employ 30–40 nm spherical gold nanoparticles (AuNPs) as colored labeling probes. AuNP-based strips commonly suffer from relatively low sensitivity because of the weak colorimetric signal brightness of AuNPs and a low capture rate (<5%) of AuNP probes at the test (T) line.[6] The sensitivity of conventional AuNP-based strip nanobiosensors is ≈3 orders of magnitude lower than that of common laboratory-based diagnostic techniques, which are far beyond the clinically relevant ranges of most biomarkers.[7] Although some signal amplification strategies, such as nanoparticle accumulation amplification,[8] metal nanoparticle growth amplification,[9] and enzymatic amplification,[10] have been developed for enhancing the detection sensitivity of strip nanobiosensors and achieved comparable sensitivity to ELISA or nucleic acid-based tests, it is still difficult to obtain satisfactory test results for the detection of disease biomarkers with low concentrations and superwide concentration ranges using these methods. In addition, these technologies cannot meet the requirements for detecting analytes with customized on-demand sensitivity.

Dr. X. Huang, Y. Zhou, Dr. Y. Leng, Dr. W. Lai, Dr. Y. Xiong
State Key Laboratory of Food Science and Technology
School of Food Science and Technology
Nanchang University
Nanchang 330047, P. R. China
E-mail: ncuskzhouyaofeng@163.com; yhxiongchen@163.com
L. Ding
Hypertension Research Institute of Jiangxi Province
Department of Cardiology
The First Affiliated Hospital of Nanchang University
Nanchang, Jiangxi 330006, P. R. China
Dr. G. Yu, Dr. X. Chen
Laboratory of Molecular Imaging and Nanomedicine (LOMIN)
National Institute of Biomedical Imaging and Bioengineering (NIBIB)
National Institutes of Health (NIH)
Bethesda, MD 20892, USA
E-mail: shawn.chen@nih.gov
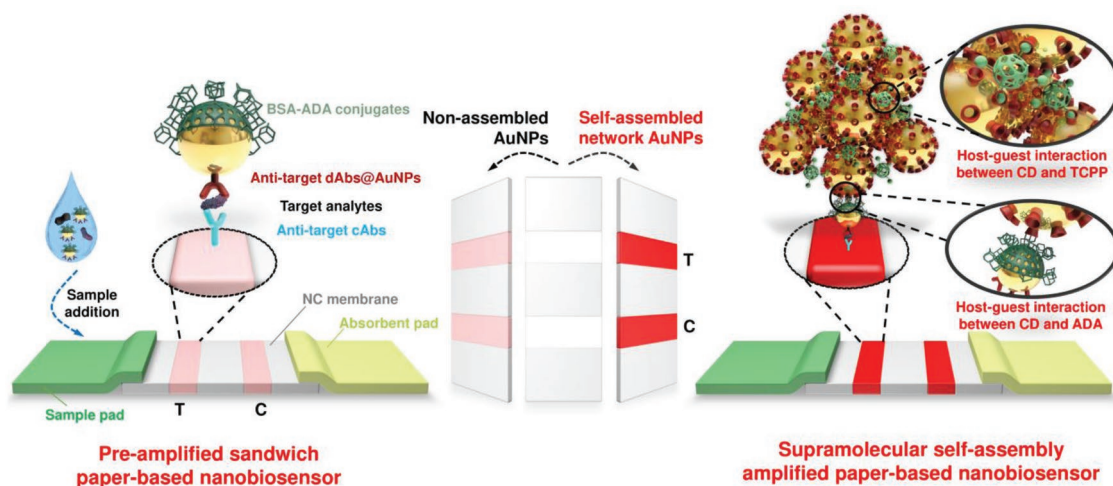
Scheme 1. Schematic representation of the design and fabrication of supramolecular self-assembly amplified strip nanobiosensor.

Recently, supramolecular recognitions based on host–guest molecular pairs have been exploited in diverse applications, including bioimaging and biosensing technologies.[11] Compared with the extensively used biotin–avidin pairs, the interaction between the host–guest pairs is relatively weak,[11c] which contributes to avoiding the nonspecific absorption originating from the high affinity of biotin–avidin pairs in the self-assembly-mediated multiple rounds of signal amplification.[12] Herein, for the first time, the supramolecular interaction between β-cyclodextrin (β-CD) and adamantane (ADA) or tetrakis(4-carboxyphenyl)porphyrin (TCPP) was designed as a smart assembly strategy to induce the layer-by-layer self-assembly of AuNPs for the increased AuNP accumulation around a target analyte (**Scheme 1**). With the selective layer-by-layer deposition of AuNPs at the T area of strip nanobiosensors, undetectable target binding molecular events can be efficiently transduced and amplified via several rounds of self-assembled AuNP accumulation. The selective AuNP assembly with supramolecular recognition can effectively suppress the nonspecific adsorption of signal-amplifying probes to surmount background signal issues, which are often observed in biotin–avidin-amplified methods, particularly multiple rounds of signal amplification. Under optimized conditions, the proposed strip nanobiosensor provided a sensitive detection for target biomarkers with the LOD of subattogram levels after six or seven rounds of AuNP self-assembly amplification (approximately dozens of molecules per strip). Besides, our amplified strip nanobiosensor shared a wide dynamic detection range of seven orders of magnitude, which could cover the clinically relevant ranges of various biomarkers. More importantly, our proposed supramolecular self-assembly-mediated signal amplification strategy provided a smart diagnostic platform for customized biomarker detection by controlling the rounds of the layer-by-layer self-assembly of AuNPs in accordance with the on-demand needs of clinicians. In short, such sensitive strategies can be applied to dynamically monitor changes in the concentrations of biomarkers from patients, but also to discover novel disease biomarkers.

2. Results and Discussion

2.1. Layer-by-Layer Self-Assembly-Mediated AuNP Accumulation Signal Amplification

The principle of layer-by-layer self-assembly-mediated AuNP accumulation signal amplification depends on the host–guest interactions between CD@AuNPs and ADA or TCPP. To validate this concept, CD@AuNPs were synthesized by using a previously reported method.[13] The maximum absorption peak of CD@AuNPs centered at 520 nm with a hydrodynamic diameter (D_H) of 20 nm (Figure S1, Supporting Information). The citrate-coated AuNPs were prepared according to a citrate reduction method[14] and then blocked with BSA-ADA conjugates (AuNP@BSA-ADA). The maximum absorption peak of the AuNP@BSA-ADA probes showed a slight redshift from 521 to 527 nm. Dynamic light scattering (DLS) analysis revealed that D_H of AuNP@BSA-ADA enlarged from 32 to 50 nm, and zeta potential increased from −45.2 to −29.8 mV (Figure S2, Supporting Information). These results indicated that BSA-ADA was successfully coupled on the surface of citrate-coated AuNPs. The resultant AuNP@BSA-ADA was then sprayed on the NC membrane as a T line. Three control groups of AuNP@BSA-ADA (control 1), BSA-coated AuNPs (AuNP@BSA, control 2), and BSA (control 3) were conducted for direct comparison (**Figure 1**a). The four prepared strips were incubated with CD@AuNPs or AuNP@BSA, and CD@AuNPs were specifically assembled onto the AuNP@BSA-ADA surface through the host–guest interaction between CD and ADA. The TCPP was used to realize the continuous signal amplification and to induce the layer-by-layer self-assembly of CD@AuNPs on the strip because each TCPP molecule contains four symmetrical carboxyphenyl subunits that can act as a scaffold to assemble CD@AuNPs. Therefore, after the strip was washed, the reacted strips were further incubated with TCPP and CD@AuNPs in an aqueous solution. The procedure was repeated by the successive addition of TCPP and CD@AuNPs (Figure 1a). The results indicated that CD@AuNPs assembled layer-by-layer onto the T line zone of the strip by using the TCPP-induced
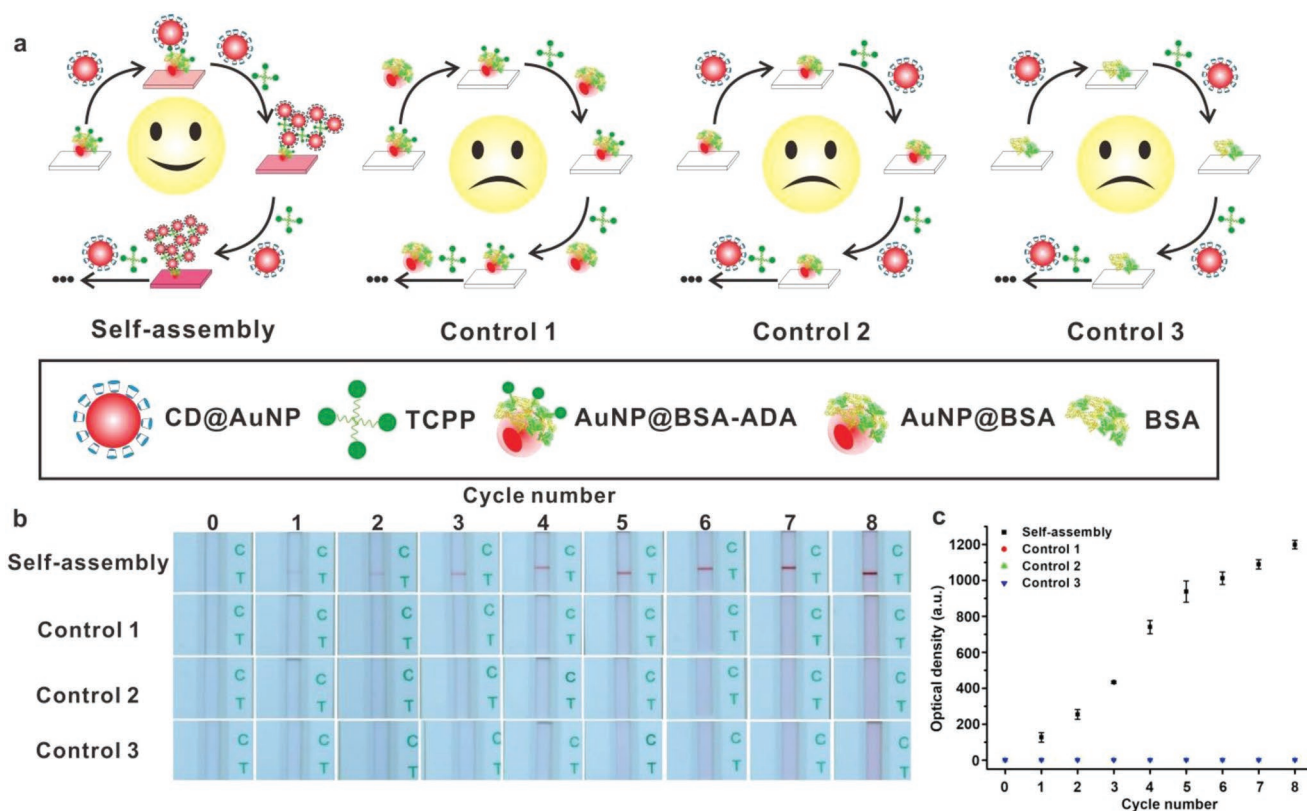
Figure 1. Characterization of AuNP@BSA-ADA and CD@AuNP pair-mediated layer-by-layer self-assembly of AuNPs to form network nanoparticles at the NC membrane through supramolecular recognition. a) Schematic representation of supramolecular AuNP self-assembly onto different decorated membrane surfaces by repeat CD@AuNP incubation cycles, including AuNP@BSA-ADA membrane surface and CD@AuNP pair (self-assembly), AuNP@BSA-ADA membrane surface and AuNP@BSA pair (control 1), AuNP@BSA membrane surface and CD@AuNP pair (control 2), as well as BSA membrane surface and CD@AuNP pair (control 3). b) The prototype images of four NC membrane surfaces after each CD@AuNP assembly incubation cycle from 0 to 8 with the AuNP@BSA-ADA and CD@AuNP pair (self-assembly) on the first row, the AuNP@BSA-ADA and AuNP@BSA pair (control 1) on the second row, the AuNP@BSA and CD@AuNP pair (control 2) on the third row, and the BSA and CD@AuNP pair (control 3) on the fourth row. c) Plots of the OD values recorded from (b) versus the number of CD@AuNP incubation cycle for self-assembly, control 1, control 2, and control 3.

self-assembly of CD@AuNPs as the repeat incubation cycles of TCPP and CD@AuNPs were conducted, thus producing the continuously deepened red bands at the T line (the first row in Figure 1b). However, when AuNP@BSA was used to replace CD@AuNPs for the repeated incubation cycle with AuNP@BSA-ADA, no red bands were observed (the second row in Figure 1b). Similar phenomena without the presence of red bands were observed in the two other control groups of AuNP@BSA or BSA (the third and fourth rows in Figure 1b). These observations suggested no nonspecific binding of CD@AuNPs on the strip in the absence of AuNP@BSA-ADA, contributing to a low background signal. Furthermore, the OD values at the T line after each cycle of signal amplification were recorded by a strip reader, and the OD values of the T line on the strip against the incubation cycle numbers were plotted for all four trials. Figure 1c indicates that AuNP@BSA-ADA and CD@AuNP pairs displayed increased OD values over the repeated incubation cycles of CD@AuNPs, whereas no changes in the OD values were obtained in the three other control cases of the AuNP@BSA-ADA and BSA@AuNP pair, the AuNP@BSA and CD@AuNP pair, and the BSA and CD@AuNP pair. This result demonstrated the successful layer-by-layer assembly

of CD@AuNPs via the supramolecular binding between CD and ADA or CD and TCPP and the high selectivity of ADA for the specific binding of CD@AuNPs over nonspecific adsorption. An excellent linear dependency between the OD values recorded after each incubation cycle and the cycle number was obtained (Figure 1c), indicating the feasibility of our designed host–guest recognition-triggered self-assembly signal amplification for the accurate quantitative detection of target analytes. In summary, the supramolecular self-assembly strategy could serve as a smart platform to produce highly specific and meaningful AuNP accumulation signal amplification.

2.2. Self-Assembly-Mediated Signal Amplification for Customized Carcinoembryonic Antigen (CEA) Detection

Encouragingly, the designed layer-by-layer self-assembly signal amplification strategy was then integrated with the common strip nanobiosensor platform for realizing the customized detection of CEA, a well-accepted biomarker for early cancer diagnosis.[15] As depicted in **Figure 2**a, the CEA molecule in the sample solution was first bound to AuNP@BSA-ADA@mAbs

ADVANCED
SCIENCE NEWS
www.advancedsciencenews.com

NANO · MICRO
small
www.small-journal.com

to form a complex. The formed complex was then captured by anti-CEA cAbs on the T line of the strip. After running the strip with the sample solution, the strip was further treated with CD@AuNPs that were used as a skeleton to trigger the AuNP assembly because of their highly specific host–guest interaction with ADA or TCPP. Consequently, at such a successive AuNP self-assembly, target analyte binding events occurred on the T lines could be efficiently transduced and magnified by the assembled AuNP accumulation, ensuring an increased detection sensitivity. To maximize this supramolecular self-assembly-mediated signal amplification efficiency for achieving the best sensitivity for CEA detection on the strip nanobiosensor, several key factors, including the coupling ratio of ADA on BSA, the labeled ratio of BSA-ADA and anti-CEA dAbs on the citrate-coated AuNP surface, and the concentration of TCPP and CD@AuNPs for triggering the self-assembly of CD@AuNPs, were systematically investigated and optimized. As shown in Figure S3 (Supporting Information), the optimized parameter combinations were summarized as follows: the labeling ratio of ADA on BSA at 60:1 (Figure S3a, Supporting Information), the labeled ratio of BSA-ADA and anti-CEA dAbs on AuNP surface at 6:4 (v/v) (Figure S3b, Supporting Information), as well as the concentrations of TCPP and CD@AuNPs at 3.5×10^{-6} and 35×10^{-12} M (Figure S3c, Supporting Information). At the meantime, the content of AuNP@BSA-ADA@mAbs and the concentration of anti-CEA cAbs on the T line were further optimized via a similar "chessboard titration" method. Table S1 (Supporting Information) indicates the optimal combinations: 1 mg mL^{-1} of

anti-CEA cAbs were spotted on the NC membrane as a T line, and 2 µL of AuNP@BSA-ADA@mAbs (35×10^{-12} M) was incubated with 78 µL of 1% HSA sample solution for 3 min, and then added to the sample well for the strip test. Under the optimized conditions, the LOD of the strip before the self-assembly signal amplification reached 0.5 ng mL^{-1} by a strip reader.

To further determine the sensitivity of the strip after signal amplification, a series of CEA sample solutions with concentrations ranging from 0 to 50 ng mL^{-1} were detected using our designed strip nanobiosensor. As described in Figure S4 (Supporting Information), without the CD@AuNP self-assembly amplification, the color intensities of the T lines gradually increased as the concentrations of the target CEA increased, showing target concentration-dependent colorimetric signal changes. The color intensities of the T lines also gradually increased as the incubation cycle of CD@AuNPs increased. Meanwhile, all the strips exhibited distinct red bands at the C lines, and the colors of the C lines deepened with the cyclic repetition of CD@AuNP self-assembly, revealing that the fabricated strips and the self-assembly signal amplification strategy were valid. Notably, no red bands at the T lines were observed at 0 ng mL^{-1} CEA even after the continuous CD@AuNP assembly, indicating that the appearance of the red band on the T line of the strips strictly depended on the specific immunorecognition between the target antigen and the capture antibody pre-immobilized on the T line rather than the nonspecific binding of CD@AuNPs. To confirm the incubation cycle-dependent AuNP accumulation at the
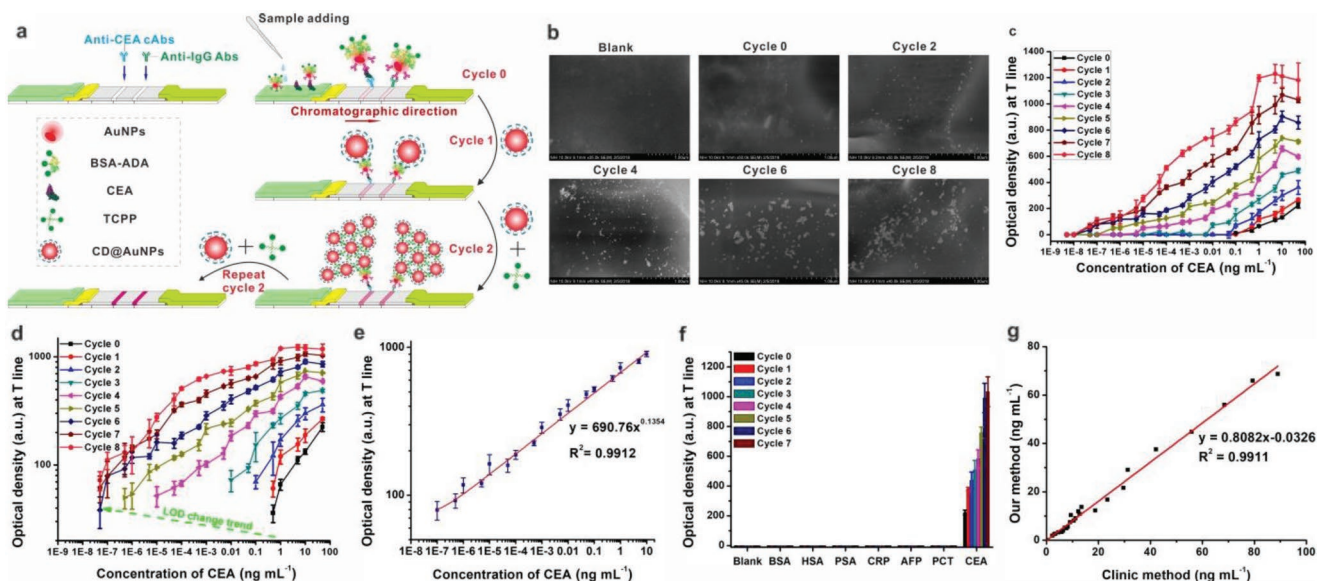

Figure 2. Supramolecular recognition-based layer-by-layer self-assembly-mediated signal amplification for the sensitive and customized detection of CEA in serum. a) Schematic representation of the customized CEA detection by using our supramolecular self-assembly-amplified strip nanobiosensor. b) SEM images verifying the AuNP accumulation at the T line of the assembled CD@AuNP after different cycle numbers, including Cycles 0, 2, 4, 6, and 8 and blank NC membrane as a control. c) Variation in the OD values at the T line against the CEA concentration in 1% HSA serum sample solution after eight CD@AuNP incubation cycles. d) The LOD change trend for CEA detection over the number of CD@AuNP incubation cycle. e) Linear response for CEA detection at the concentration ranging from 0.1 fg mL^{-1} to 10 ng mL^{-1} under six runs of CD@AuNP incubation cycle. f) Selectivity evaluation of our amplified strip nanobiosensor by determining the signal responses against several common protein biomarkers in serum, including CEA (50 ng mL^{-1}) and other nontargets of BSA, HSA, PSA, CRP, AFP, and PCT at 500 ng mL^{-1}. g) Correlation analysis of the measured CEA concentrations between our self-assembly amplified strip nanobiosensor and the clinically used CEA chemiluminescence assay kits in 26 human serum samples with target concentrations ranging from 0 to 89.1 ng mL^{-1}.

T lines, the blank NC membrane and five positive T bands from cycles 0, 2, 4, 6, and 8 were observed through scanning electron microscopy (SEM) imaging after the assembled strip detected the sample at 10 ng mL^{-1} CEA. Figure 2b reveals that no AuNPs were found in the blank NC membrane. By contrast, a small number of AuNPs were seen on the T band from cycle 0, indicating that the target CEA could induce the successful capture of AuNP@BSA-ADA@mAbs at the T line. Furthermore, the number of AuNPs on the T bands increased as the incubation cycle of CD@AuNPs increased, suggesting an effective target induced AuNP accumulation at the T line via self-assembly. These phenomena demonstrated that the presence of the targets could induce the specific capture of AuNP@BSA-ADA@mAbs at the T lines, and then the captured AuNP@BSA-ADA@mAbs could serve as a selective framework for the specific self-assembly of CD@AuNPs over non-specific adsorption, which was essential for the CD@AuNP signal amplification through supramolecular self-assembly in the actual analysis application to remove background signals.

The OD values at the T and C lines after each incubation cycle of CD@AuNPs were then recorded with a strip reader to obtain the customized detection of CEA in the spiked HSA sample solution. Figure 2c indicates that the OD values at the T lines increased with the CEA concentrations and the number of CD@AuNP assembly cycles. The LOD of our strip nanobiosensor after each CD@AuNP incubation cycle is defined as the lowest CEA concentration to yield an OD value greater than that obtained from the negative control (OD$_{Control}$ = 0). Accordingly, the LOD values after each self-assembly cycle amplification were reduced from 0.5 ng mL^{-1} to 0.1 fg mL^{-1} against the repeated CD@AuNP incubation cycle, and the lowest LOD reached 0.1 fg mL^{-1} after six CD@AuNP assembly cycles (marked as cycle 6 in Figure 2d). The added volume of the CEA sample solution was 78 µL, and the LOD indicated that ≈23 CEA molecules per strip were detectable by using our proposed strategy. This value was approximately six orders of magnitude lower than that of the conventional AuNP-based strip without amplification (0.5 ng mL^{-1}, Figure S5, Supporting Information). Our method was also several orders of magnitude more sensitive than those of conventional CEA ELISA method and other reported immunoassay-based methods (Table S4, Supporting Information). It should be emphasized that the LOD of the proposed method under no cycle amplification reached 0.5 ng mL^{-1}, which was tenfold lower than the clinical cutoff of 5.0 ng mL^{-1} (a potential cancer risk).[16] This result suggested that our approach could serve as a rapid screening tool within 15 min with an LOD comparable with that of conventional ELISA. The monitoring of the CEA level in the serum is also crucial to evaluate the treatment efficacy and prognosis and to monitor the recurrence and metastasis of cancer.[17] However, in these cases, the CEA occurs in serum in such trace amounts and is difficult to detect by using conventional analytical tools. Alternatively, our method could provide a high sensitivity of 10 pg mL^{-1} after four CD@AuNP assembly cycles (marked as cycle 4 in Figures S4 and S6, Supporting Information), which could achieve the trace detection of target CEA. Furthermore, only less than 90 min was required, that is, less than or equal to the total analysis time required to complete traditional ELISA. The lower CEA concentration in the serum should be measured by simply increasing the number of CD@AuNP incubation cycles. Our amplified strip nanobiosensor shared a broad linear detection range from 0.1 fg mL^{-1} to 10 ng mL^{-1} with a correlation coefficient (R^2) greater than 0.9912 (Figure 2e). The wide linear detection range contrasted strikingly with that of conventional CEA ELISA (1 to 50 ng mL^{-1}) and was suitable for simple and rapid target determination without any dilution and enrichment step. Collectively, the layer-by-layer CD@AuNP assembly-modulated signal amplification strategy provided a smart analytical platform for the customized target detection to match the requirement of the "customized sensitivity" in actual applications.

Furthermore, a series of continuously 100-fold diluted serum sample solutions with CEA concentrations at 200 ng mL^{-1}, 2 ng mL^{-1}, 20 pg mL^{-1}, 200 fg mL^{-1}, 2 fg mL^{-1}, 0.2 fg mL^{-1}, and 0 fg mL^{-1} were analyzed with our method to explore the feasibility of our fabricated method for determining the presence of targets at different concentration levels. For each CEA concentration, the standard for stopping the CD@AuNP incubation cycle was the appearance of a positive red band on the T line of the test strip, and the corresponding OD value was recorded via a strip reader. In Table S2 (Supporting Information), when the CEA concentrations were 200 and 2 ng mL^{-1}, the sample solutions could be detected directly on the basis of our reported method without CD@AuNP assembly cycles. When the CEA concentration was reduced to 20 pg mL^{-1}, the serum sample solution could be detected after three CD@AuNP assembly cycles. As the CEA concentration continuously decreased to 200 fg mL^{-1} or lower, more CD@AuNP assembly cycles were required to achieve the positive detection. By contrast, no OD values at the T line were collected on a strip reader in the CEA-negative serum sample solution even after six CD@AuNP assembly cycles. These results further confirmed that our designed layer-by-layer CD@AuNP assembly technology could provide a sensitive and reliable detection at different CEA concentrations with or without CD@AuNP assembly cycles.

The selectivity of our proposed strip nanobiosensors before and after the assembly amplification was investigated by determining the responses against several common protein biomarkers in the serum, including CEA (50 ng mL^{-1}), and other nontargets (BSA, HSA, PSA, CRP, AFP, and PCT) at 500 ng mL^{-1}. A blank sample solution was set as a negative control. The strip prototypes of the responses and the corresponding OD values at the T lines are displayed in Figure S7 (Supporting Information) and Figure 2f. The results indicated that a red band that deepened gradually and the corresponding increase in OD values on the T lines of the strip over the repeated CD@AuNP assembly cycle were observed in the testing CEA-positive samples, whereas no similar responses were observed to measure other proteins and blank control. This finding demonstrated an excellent selectivity of our technology against target CEA. Encouragingly, our strip nanobiosensor by using the CD@AuNP assembly cycle amplification was further extended for the sensitive and specific detection of CEA in the blood samples from patients with cancer. A correlation analysis was conducted between our self-assembly-amplified method and the clinically used CEA chemiluminescence assay kits in 26 human serum samples to estimate the practicability

and reliability. In Figure S8 (Supporting Information), 25 samples were detected as CEA positive by using our method and the commercial kits. Furthermore, one sample was measured to be CEA negative by both methods. Figure 2g shows that the detection results obtained from the two methods had a high linear correlation with an R^2 of 0.9911, indicating that our CD@AuNP assembly-based signal amplification for the strip nanobiosensor functioned reasonably robust in actual biomarker detection from complex biological media.

2.3. Self-Assembly Amplified Strip Nanobiosensors for Customized p24 Detection

To evaluate the universality of our designed signal amplification, the amplified strip nanobiosensor was further extended to measure HIV-1 capsid p24 antigen, the earliest protein biomarker post HIV infection.[10c] The sensitive and early detection of the p24 antigen in the serum could largely shorten the window period of the early detection of acute HIV infection that always challenges conventional HIV antibody assays (≈28 d after infection).[18] The reduced window period contributed to accurate early diagnosis, promoted timely intervention, and decreased HIV virus transmission.[19] However, in most HIV cases, the clinically relevant concentration ranges of p24 antigen during acute HIV infection were far less than the reported LOD values of these leading colorimetric strip nanobiosensors (≈10–15 pg mL^{-1}) that were mainly limited by the weak absorbance of the labeled probes.[20] Thus, a high detection sensitivity and a wide detection range previously unrealizable in conventional strip nanobiosensors were demonstrated through the integration of our designed

self-assembly signal amplification platform into AuNP-based lateral flow strip architecture. Similar to the amplified CEA strip immunosensor, the classical sandwich strip nanobiosensor was developed using the p24 antibody pair to replace the CEA antibody pair for target recognition and to detect HIV p24 antigen. The layer-by-layer CD@AuNP accumulation amplification step through the supramolecular self-assembly was unified for both targets as presented in **Figure 3**a. Figure S9 (Supporting Information) presents the detailed results for the sensitive detection of p24 antigen in spiked serum with our amplified strip nanobiosensor, and the results showed p24 concentration-dependent changes in color at the T lines of the strips. As the number of incubation cycles of CD@AuNPs increased, the color intensity of the T lines significantly increased. Further quantitative analysis was conducted by recording the OD values on the T lines of the strip against p24 concentration after each self-assembly amplification. In Figure 3b, the OD values at the T lines increased as the p24 concentrations and the number of incubation cycles increased, and the corresponding LOD values of our amplified strip nanobiosensor after each self-assembly cycle amplification significantly decreased from 0.5 ng mL^{-1} to 0.01 fg mL^{-1} against the number of CD@AuNP incubation cycles. The lowest LOD was 0.01 fg mL^{-1} (≈18 p24 molecules per strip) under six runs of incubation cycle (Figure 3c and Figure S10, Supporting Information), which was seven orders of magnitude lower than that of the AuNP-based strip without cyclic self-assembly amplification (0.5 ng mL^{-1}, Figure S11, Supporting Information). To the best of our knowledge, the LOD value for p24 was the lowest among the currently available strip nanobiosensors (Table S4, Supporting Information) and approached the sensitivity of the well-accepted nucleic acid-based "gold standard" method. This
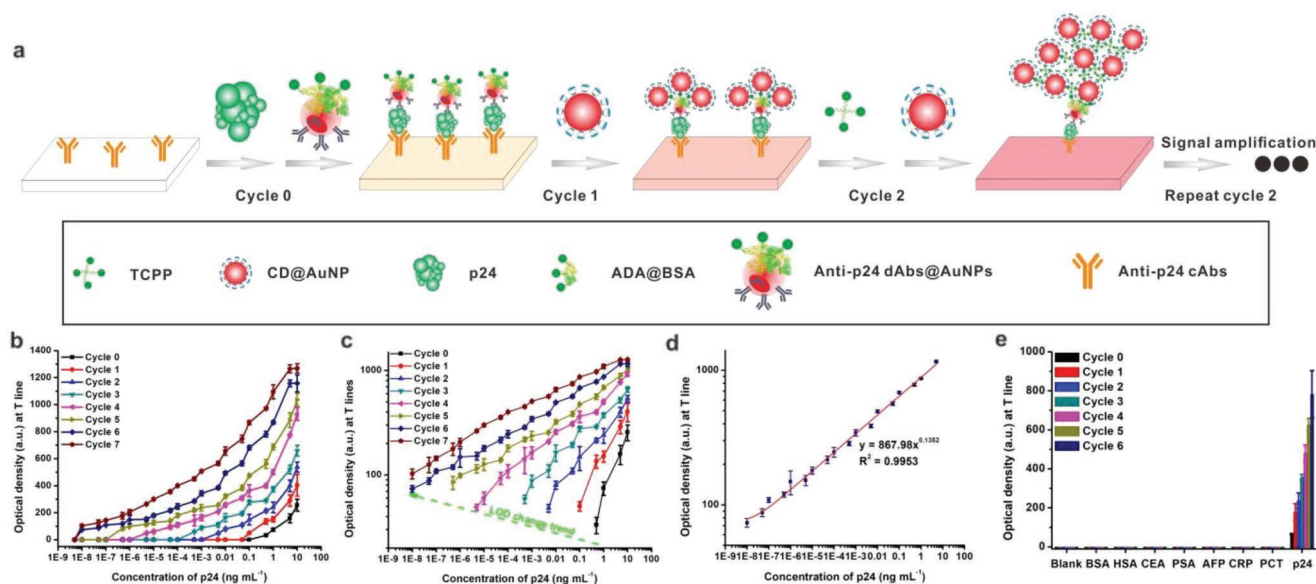

Figure 3. Application of layer-by-layer self-assembly-mediated signal amplification in the sensitive and customized detection of p24 in serum. a) Schematic representation of p24 detection by using our amplified strip nanobiosensor. b) Variation in the OD values at the T line against the concentrations of p24 antigen after seven CD@AuNP incubation cycles. c) LOD change trend for p24 determination versus the number of CD@AuNP incubation cycle. d) Linear response with R^2 = 0.9953 for p24 detection with the concentration ranging from 0.01 fg mL^{-1} to 5 ng mL^{-1} after six CD@AuNP incubation cycles. e) Specificity analysis of our amplified strip nanobiosensor by recording the responses against several serum protein biomarkers, including p24 at 5 ng mL^{-1}, and other commen interfered proteins of BSA, HSA, CEA, PSA, AFP, CRP, and PCT at 500 ng mL^{-1}.

result indicated that our amplified strip nanobiosensor could become a promising alternative to the expensive nucleic acid detection for the early diagnosis of acute HIV infection in clinics. Figure 3d indicates that an excellent linear correlation with R^2 of 0.9953 was achieved between the OD values at the T line and the concentrations of p24 antigen after six CD@AuNP incubation cycles, and the dynamic detection covered approximately eight orders of magnitude target concentration ranging from 0.01 fg mL^{-1} to 5 ng mL^{-1}, which could match the p24 antigen detection at different concentrations at different HIV infective stages. Further "customized" detection at different concentrations of p24 antigens ranging from 0.025 fg mL^{-1} to 10 ng mL^{-1} was performed using the same analytical protocol as CEA. In Table S3 (Supporting Information), the spiked serum samples were directly detectable without self-assembly amplification when p24 concentrations were more than 0.5 ng mL^{-1}. By contrast, the spiked serum samples with p24 concentrations of below 0.5 ng mL^{-1} could be detected with an additional self-assembly amplification step and increasing incubation cycles of CD@AuNP to match the successful detection of p24 with decreased p24 concentrations. Notably, after six CD@AuNP self-assembly cycles, all p24-spiked serum samples could be successfully discovered with positive signals, whereas the p24-negative serum samples could not produce a similar response even after six runs of self-assembly cycles. Moreover, further selectivity analysis in Figure 3e displayed that our amplified strip nanobiosensor possessed outstanding discrimination capacities for p24 antigen compared with other common serum protein biomarkers. These findings demonstrated a highly sensitive and specific molecular recognition of our amplified method to p24 antigen in the serum, providing huge promise for the early diagnosis of HIV infection in resource-limited settings.

3. Conclusion

Herein, we describe a smart cyclic signal amplification strategy for effectively transducing and amplifying the undetected target binding molecular events on the paper-based strip nanobiosensor by using supramolecular self-assembly. The amplified nanobiosensor demonstrates its potential and universality in clinically significant ranges for CEA and p24 detection in spiked serum and detection of CEA in clinical samples of patients with cancer. We achieved high detection sensitivity of subattogram level, an LOD of dozens of copies per strip, and share an extremely wide dynamic linear detection range for concentration over seven orders of magnitude, which can cover the clinically relevant ranges of various biomarkers. In particular, cyclic incubation-modulated signal amplification modes provide the possibility to realize customized biomarker detection, along with the on-demand needs of clinicians, such as early diagnosis, dynamic monitoring, and prognosis evaluation. In combination with microfluidic chip approaches, we can anticipate that the designed layer-by-layer self-assembly-amplified strip nanobiosensor will provide several enhanced performances, including analysis speed, reproducibility, and detection throughput, thereby further expanding its applications.

Supporting Information

Supporting Information is available from the Wiley Online Library or from the author.

Conflict of Interest

The authors declare no conflict of interest.

[1] a) A. B. Chinen, C. M. Guan, J. R. Ferrer, S. N. Barnaby, T. J. Merkel, C. A. Mirkin, *Chem. Rev.* **2015**, *115*, 10530; b) L. Wu, X. Qu, *Chem. Soc. Rev.* **2015**, *44*, 2963; c) M. Swierczewska, G. Liu, S. Lee, X. Chen, *Chem. Soc. Rev.* **2012**, *41*, 2641; d) X. Huang, Y. Liu, B. Yung, Y. Xiong, X. Chen, *ACS Nano* **2017**, *11*, 5238; e) Y. Song, Y.-Y. Huang, X. Liu, X. Zhang, M. Ferrari, L. Qin, *Trends Biotechnol.* **2014**, *32*, 132; f) C. He, S. Zheng, Y. Luo, B. Wang, *Theranostics* **2018**, *8*, 237.

[2] a) R. Etzioni, N. Urban, S. Ramsey, M. McIntosh, S. Schwartz, B. Reid, J. Radich, G. Anderson, L. Hartwell, *Nat. Rev. Cancer* **2003**, *3*, 243; b) W. Zhou, X. Gao, D. Liu, X. Chen, *Chem. Rev.* **2015**, *115*, 10575; c) Y. Zhang, X. Mi, X. Tan, R. Xiang, *Theranostics* **2019**, *9*, 491; d) S. K. Vashist, P. B. Luppa, L. Y. Yeo, A. Ozcan, J. H. T. Luong, *Trends Biotechnol.* **2015**, *33*, 692.

[3] a) A. J. Steckl, P. Ray, *ACS Sens.* **2018**, *3*, 2025; b) A. P. Drabovich, V. Okhonin, M. Berezovski, S. N. Krylov, *J. Am. Chem. Soc.* **2007**, *129*, 7260; c) A. Vallée-Bélisle, F. Ricci, K. W. Plaxco, *J. Am. Chem. Soc.* **2012**, *134*, 2876; d) A. Porchetta, A. Vallée-Bélisle, K. W. Plaxco, F. Ricci, *J. Am. Chem. Soc.* **2012**, *134*, 20601; e) X. Zhang, X. Lou, F. Xia, *Theranostics* **2017**, *7*, 1847.

[4] D. Kang, A. Vallée-Bélisle, A. Porchetta, K. W. Plaxco, F. Ricci, *Angew. Chem., Int. Ed.* **2012**, *51*, 6717.

[5] a) C. Parolo, A. Merkoçi, *Chem. Soc. Rev.* **2013**, *42*, 450; b) M. Yang, W. Zhang, J. Yang, B. Hu, F. Cao, W. Zheng, Y. Chen, X. Jiang, *Sci. Adv.* **2017**, *3*, eaao4862; c) H. de Puig, I. Bosch, L. Gehrke, K. Hamad-Schifferli, *Trends Biotechnol.* **2017**, *35*, 1169; d) V. Tran, B. Walkenfort, M. König, M. Salehi, S. Schlücker, *Angew. Chem.,*

ADVANCED
SCIENCE NEWS

www.advancedsciencenews.com

NANO · MICRO

small

www.small-journal.com

Int. Ed. **2019**, *58*, 442; e) J. Li, M. A. Baird, M. A. Davis, W. Tai, L. S. Zweifel, K. M. A. Waldorf, M. Gale Jr., L. Rajagopal, R. H. Pierce, X. Gao, *Nat. Biomed. Eng.* **2017**, *1*, 0082; f) L. Hong, K. Wang, W. Yan, H. Xu, Q. Chen, Y. Zhang, D. Cui, Q. Jin, J. He, *Theranostics* **2018**, *8*, 6121.

[6] a) X. Huang, Z. P. Aguilar, H. Xu, W. Lai, Y. Xiong, *Biosens. Bioelectron.* **2016**, *75*, 166; b) Y. Zhou, L. Ding, Y. Wu, X. Huang, W. Lai, Y. Xiong, *TrAC, Trends Anal. Chem.* **2019**, *112*, 147; c) L. Zhan, S.-z. Guo, F. Song, Y. Gong, F. Xu, D. R. Boulware, M. C. McAlpine, W. C. W. Chan, J. C. Bischof, *Nano Lett.* **2017**, *17*, 7207.

[7] J. Hu, S. Wang, L. Wang, F. Li, B. Pingguan-Murphy, T. J. Lu, F. Xu, *Biosens. Bioelectron.* **2014**, *54*, 585.

[8] a) R. Chapman, Y. Lin, M. Burnapp, A. Bentham, D. Hillier, A. Zabron, S. Khan, M. Tyreman, M. M. Stevens, *ACS Nano* **2015**, *9*, 2565; b) J. Liu, D. Mazumdar, Y. Lu, *Angew. Chem., Int. Ed.* **2006**, *45*, 7955; *Angew. Chem.* **2006**, *118*, 8123.

[9] a) S. K. Rastogi, C. M. Gibson, J. R. Branen, D. E. Aston, A. L. Branen, P. J. Hrdlicka, *Chem. Commun.* **2012**, *48*, 7714; b) W. Yang, X.-B. Li, G.-W. Liu, B.-B. Zhang, Y. Zhang, T. Kong, J.-J. Tang, D.-N. Li, Z. Wang, *Biosens. Bioelectron.* **2011**, *26*, 3710.

[10] a) B. Jiang, D. Duan, L. Gao, M. Zhou, K. Fan, Y. Tang, J. Xi, Y. Bi, Z. Tong, G. F. Gao, N. Xie, A. Tang, G. Nie, M. Liang, X. Yan, *Nat. Protoc.* **2018**, *13*, 1506; b) Y. Zhao, M. Yang, Q. Fu, H. Ouyang, W. Wen, Y. Song, C. Zhu, Y. Lin, D. Du, *Anal. Chem.* **2018**, *90*, 7391; c) C. N. Loynachan, M. R. Thomas, E. R. Gray, D. A. Richards, J. Kim, B. S. Miller, J. C. Brookes, S. Agarwal, V. Chudasama, R. A. McKendry, M. M. Stevens, *ACS Nano* **2018**, *12*, 279; d) Z. Gao, H. Ye, D. Tang, J. Tao, S. Habibi, A. Minerick, D. Tang, X. Xia, *Nano Lett.* **2017**, *17*, 5572.

[11] a) Y. Guo, S. Guo, J. Ren, Y. Zhai, S. Dong, E. Wang, *ACS Nano* **2010**, *4*, 4001; b) G. Yu, K. Jie, F. Huang, *Chem. Rev.* **2015**, *115*, 7240; c) D. Shetty, J. K. Khedkar, K. M. Park, K. Kim, *Chem. Soc. Rev.* **2015**, *44*, 8747; d) M. Li, A. Lee, K. L. Kim, J. Murray, A. Shrinidhi,

G. Sung, K. M. Park, K. Kim, *Angew. Chem.* **2018**, *130*, 2142; e) H. Cai, Y.-L. Huang, D. Li, *Coord. Chem. Rev.* **2019**, *378*, 207; f) G. Yu, X. Chen, *Theranostics* **2019**, *9*, 3041; g) K. L. Kim, G. Sung, J. Sim, J. Murray, M. Li, A. Lee, A. Shrinidhi, K. M. Park, K. Kim, *Nat. Commun.* **2018**, *9*, 1712.

[12] J. Park, Y. Park, S. Kim, *ACS Nano* **2013**, *7*, 9416.

[13] Y. Zhao, Y. Huang, H. Zhu, Q. Zhu, Y. Xia, *J. Am. Chem. Soc.* **2016**, *138*, 16645.

[14] X. Huang, Z. Xu, Y. Mao, Y. Ji, H. Xu, Y. Xiong, Y. Li, *Biosens. Bioelectron.* **2015**, *66*, 184.

[15] a) H. J. Hansen, J. J. Snyder, E. Miller, J. P. Vandevoorde, O. N. Miller, L. R. Hines, J. J. Burns, *Hum. Pathol.* **1974**, *5*, 139; b) B. Liu, Y. Li, H. Wan, L. Wang, W. Xu, S. Zhu, Y. Liang, B. Zhang, J. Lou, H. Dai, K. Qian, *Adv. Funct. Mater.* **2016**, *26*, 7994; c) H. Lee, Y. Jang, S. Park, H. Jang, E. J. Park, H. J. Kim, H. Kim, *Theranostics* **2018**, *8*, 4247.

[16] Y. Chen, J. Sun, Y. Xianyu, B. Yin, Y. Niu, S. Wang, F. Cao, X. Zhang, Y. Wang, X. Jiang, *Nanoscale* **2016**, *8*, 15205.

[17] J. A. Ludwig, J. N. Weinstein, *Nat. Rev. Cancer* **2005**, *5*, 845.

[18] a) S. Tang, I. Hewlett, *J. Infect. Dis.* **2010**, *201*, S59; b) B. M. Branson, J. D. Stekler, *J. Infect. Dis.* **2012**, *205*, 521; c) N. E. Rosenberg, C. D. Pilcher, M. P. Busch, M. S. Cohen, *Curr. Opin. HIV AIDS* **2015**, *10*, 61.

[19] a) S. E. Rutstein, J. Ananworanich, S. Fidler, C. Johnson, E. J. Sanders, O. Sued, A. Saez-Cirion, C. D. Pilcher, C. Fraser, M. S. Cohen, M. Vitoria, M. Doherty, J. D. Tucker, *J. Int. AIDS Soc.* **2017**, *20*, 21579; b) H. Shafiee, S. Wang, F. Inci, M. Toy, T. J. Henrich, D. R. Kuritzkes, U. Demirci, *Annu. Rev. Med.* **2015**, *66*, 387.

[20] a) M. Miedouge, M. Grèze, A. Bailly, J. Izopet, *J. Clin. Virol.* **2011**, *50*, 57; b) L. Vallefuoco, C. Mazzarella, G. Portella, *Expert Rev. Mol. Diagn.* **2016**, *16*, 723; c) M. W. Pandori, J. Hackett, B. Louie, A. Vallari, T. Dowling, S. Liska, J. D. Klausner, *J. Clin. Microbiol.* **2009**, *47*, 2639.

1903861 (8 of 8)